applied sciences

MDPI

Article

Mechanism of Strength Development and Microstructural Evolution of KDJ-II–Cement Composite-Stabilized Soil for Loess Base Courses

Hongjuan Wu [1,2,3,*], Bangxuan Zhao [1,2,3], Xiaohui Niu [1,2,3], Rui Wang [1,2,3], Wei Zhang [1,2,3], Yanmei Tong [1,2,3] and Chenggui Chen [4]

[1] College of Civil Engineering, Northwest Minzu University, Lanzhou 730124, China; y241730885@stu.xbmu.edu.cn (B.Z.); y231730872@stu.xbmu.edu.cn (X.N.); 13659464950@163.com (R.W.); zw4241261@126.com (W.Z.); tongym@xbmu.edu.cn (Y.T.)
[2] Gansu Key Laboratory of Green Engineering Materials and Low-Carbon Construction, Lanzhou 730124, China
[3] Industrial Research Institute of Prefabricated Buildings and Energy-Saving Materials, Lanzhou 730124, China
[4] Gansu Provincial Transportation Research Institute Group Co., Ltd., Lanzhou 730030, China; 17862980373@163.com
* Correspondence: whj0116@163.com; Tel.: +86-13919065085

Abstract

Rural road construction in the loess region of Gansu Province is constrained by aggregate shortage, high material transportation costs, and the limited early performance of cement-stabilized soil. In this study, KDJ-II stabilizer and cement were used to prepare KDJ-II–cement composite-stabilized soil for potential use as a base-course material. Compared with cement-stabilized soil, the addition of 0.02% KDJ-II increased the 7-day unconfined compressive strength, splitting tensile strength, and resilient modulus by 16.7%, 17.6%, and 12.1%, respectively. Leaching-based ion concentration analysis, XRD, FTIR, and SEM were used to interpret the early strength development mechanism. The results suggest that KDJ-II influenced the leachable ion release and retention behavior of the cement-stabilized soil and helped form a sulfate-rich, alkaline, and soluble-silica-bearing reaction environment under the tested conditions. This environment may favor the development of sulfate-bearing hydration products, the activation of primary aluminosilicate minerals, and the formation of C–S–H-like gels. The coupled variations in leachable Ca^{2+}, SO_4^{2-}, and Na^+, together with the increase in calcite, decrease in albite, broadening of the absorption band at approximately 1018 cm^{-1}, and the SEM-observed needle/fibrous products, flocculent gels, and reduced visible pores, collectively support the interpretation that KDJ-II promotes particle cementation, pore filling, and microstructural densification. Overall, this study indicates that, under the selected mixture proportion and curing condition, KDJ-II can improve the early strength and stiffness of cement-stabilized loess by modifying the early reaction environment and promoting the coordinated development of hydration-related products and a denser microstructure.

Keywords: ionic stabilizer; cement-stabilized soil; composite-stabilized soil; sulfate-bearing hydration products; microstructural evolution

Academic Editor: Tiago Filipe da Silva Miranda

Received: 8 May 2026
Revised: 24 May 2026
Accepted: 3 June 2026
Published: 5 June 2026

1. Introduction

Rural road construction in the loess regions of Gansu Province faces two practical challenges: a shortage of sand and gravel aggregates and high costs for material purchase

and transportation [1]. Loess has a loose structure, strong collapsibility, poor water stability, and high sensitivity to environmental actions such as wetting–drying and freeze–thaw cycles. Therefore, it is not suitable for direct use as a base course material [2–7]. Although cement treatment can improve the engineering properties of loess and provide a certain level of strength, its stabilization effect is still limited by shrinkage cracking and poor erosion resistance [5–8]. Therefore, developing an efficient in-situ stabilization method for loess used in base courses remains an important issue in rural road engineering in loess regions.

Ionic soil stabilizers have attracted increasing attention in recent years. They can modify the interactions between pore fluid and particle surfaces, promote interparticle cementation, and reduce the water sensitivity of materials [9–11]. Previous studies have shown that the combination of ionic stabilizers and cementitious materials can improve the strength and durability-related behavior of road geotechnical materials and complex soils [12–14]. However, the effectiveness of ionic stabilizers is closely related to soil type, and their engineering applicability still needs to be verified by experiments [10,15–17]. Recent studies have further examined sustainable binders, silica-based additives, alkali/sulfate-activated systems, and cement–organic additive systems for loess or soil stabilization. These studies indicate that strength and durability improvements are closely related to hydration-product development, pore filling, ion-scale reactions, and microstructural densification [18–20]. Existing studies on loess stabilization have mainly focused on the improvement of macroscopic mechanical properties and durability evaluation. However, microscopic evidence for the internal source of performance improvement is still insufficient. In particular, for KDJ-II–cement stabilized loess, the available evidence is still insufficient to explain how the stabilizer affects early strength development beyond conventional cement hydration. Previous studies have reported improvements in mechanical properties and durability-related behavior of stabilized soils, but fewer studies have connected leachable ion behavior, crystalline phase evolution, bonding-environment changes, and SEM-observed microstructural densification within a single early-age framework. Therefore, the novelty of this study does not lie in proposing a completely new hydration product, but in establishing a multi-scale evidence chain for the selected KDJ-II–cement stabilized loess system. This evidence chain is used to interpret how the addition of KDJ-II may influence the early reaction environment, hydration-related product development, and microstructural densification under the tested conditions.

Based on this background, this study used low-plasticity loess from Dingxi, Gansu Province, as the research material. KDJ-II stabilizer and cement were used together to prepare KDJ-II–cement composite-stabilized soil. First, unconfined compressive strength, splitting tensile strength, and resilient modulus tests were conducted to evaluate the improvement in early mechanical properties. Then, ion concentration testing, X-ray diffraction (XRD), Fourier-transform infrared spectroscopy (FTIR), and scanning electron microscopy (SEM) were used to systematically analyze the strength development mechanism in terms of ion variation, product formation, and microstructural evolution. This study aims to evaluate the early strengthening effect of KDJ-II under the selected mixture proportion and to interpret its possible role in modifying the early reaction environment of cement-stabilized loess. By combining mechanical testing with leaching-based ion analysis, XRD, FTIR, and SEM, this study attempts to establish a multi-scale link among leachable ion behavior, mineral phase evolution, bonding-environment changes, microstructural densification, and early strength growth. The results provide experimental evidence for understanding the early-age behavior of KDJ-II–cement composite-stabilized soil and offer a basis for further evaluation of its application potential in rural road base courses in loess regions.

2. Materials and Methods

2.1. Stabilizer

2.1.1. Basic Physical Properties of the Stabilizer

Ionic soil stabilizers are a type of chemical admixture. They can modify the interactions between pore fluid and particle surfaces and improve the water stability and mechanical behavior of materials under certain conditions. However, their effectiveness is usually closely related to soil type and needs to be evaluated through appropriate comparative tests [9,11]. In this study, KDJ-II stabilizer was selected according to the characteristics of Gansu loess and the engineering requirements. It is a transparent and viscous liquid at room temperature. Its appearance is shown in Figure 1, and its basic properties are listed in Table 1.

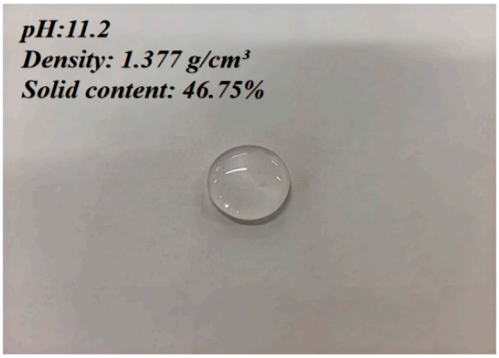

Figure 1. Appearance of the KDJ-II stabilizer.

Table 1. Basic properties of the stabilizer.

Item	Unit	Technical Specification	Measured Value
pH	/	11 ± 1.0	11.2
Density	g/cm^3	1.35 ± 0.03	1.377
Solid content	%	45 ± 2.0	46.75

2.1.2. Ion Composition Analysis of the Stabilizer Solution

To determine the main components of KDJ-II, its solution was quantitatively analyzed using an inductively coupled plasma optical emission spectrometer (ICP-OES; Agilent 730, Agilent Technologies, Santa Clara, CA, USA) and an ion chromatograph (Dionex ICS-5000, Thermo Fisher Scientific, Waltham, MA, USA). Before testing, the original KDJ-II solution was diluted by a factor of 10. The cation components were measured by ICP-OES, and the anion components were measured by ion chromatography. The measured results were then converted according to the dilution factor to obtain the concentrations in the original KDJ-II solution, as shown in Table 2.

Table 2. Main components in the KDJ-II solution.

Detected Component	Concentration (mg/L)	Anion Component	Concentration (mg/L)
Si	1430.6	SO_4^{2-}	4910.5
Na	606.2	PO_4^{3-}	346.1
Al	12.1	Cl^-	280.2
K	7.5	-	-
Fe	4.3	-	-
Ca	2.0	-	-
Mg	0.11	-	-

As shown in Table 2, SO_4^{2-} was the dominant anion in the KDJ-II solution, followed by PO_4^{3-} and Cl^-. Among the cation-related components, which were expressed as elemental concentrations by ICP-OES, Si and Na had relatively high concentrations, while Al, K, Fe, Ca, and Mg had relatively low concentrations. Overall, KDJ-II is an alkaline stabilizer solution that is rich in sulfate and silicate-related components.

2.2. Test Soil

The soil used in this study was loess collected from Dingxi, Gansu Province. Its basic physical properties are listed in Table 3. The Dingxi loess has a relatively loose particle structure. It is relatively compact in the dry state but tends to disperse after contact with water. Before testing, large soil blocks were crushed, and the maximum particle size was controlled to be less than 5 mm. The measured physical properties are shown in Table 3.

Table 3. Basic physical properties of the Dingxi loess from Gansu Province.

Item	Natural Water Content	Optimum Moisture Content	Maximum Dry Density	Liquid Limit	Plastic Limit	Plasticity Index
Value	7.8%	12.6%	1.84 g/cm^3	30%	20.1%	9.9

2.3. Cement

Qilianshan 42.5 R ordinary Portland cement was used in this study. Its initial setting time was 173 min, and its final setting time was 238 min. The 28-day flexural strength and compressive strength were 8.3 MPa and 48.8 MPa, respectively.

2.4. Specimen Preparation

The specimens were prepared according to the optimum moisture content of 12.6% and the maximum dry density of 1.84 g/cm^3, which were determined by the standard compaction test. A preliminary orthogonal proportioning test was conducted to determine the mixture used in the main comparative study. According to the orthogonal design, stabilizer content, cement content, and degree of compaction were selected as the three main factors. The investigated levels of stabilizer content were 0.015%, 0.020%, and 0.025% by dry soil mass; the cement contents were 4%, 5%, and 6% by dry soil mass; and the degrees of compaction were 93%, 95%, and 97%. An L9(3^4) orthogonal array was adopted, and the fourth column was left blank and used as the error column for the orthogonal analysis. The orthogonal design is shown in Table 4.

Table 4. Preliminary L9(3^4) orthogonal design for mixture selection.

Run	Factor Level			
	A: KDJ-II Content (%)	B: Cement Content (%)	Blank Column	C: Compaction Degree (%)
1	0.015	4	1	93
2	0.015	5	2	95
3	0.015	6	3	97
4	0.020	4	2	97
5	0.020	5	3	93
6	0.020	6	1	95
7	0.025	4	3	95
8	0.025	5	1	97
9	0.025	6	2	93

Note: The blank column was used as the error column in the orthogonal analysis.

The 7-day unconfined compressive strength and 7-day splitting tensile strength were used as the main optimization indicators because they reflect the early load-bearing capacity and cracking resistance of stabilized soil for base-course applications. Based on the range analysis and analysis of variance of the preliminary test results, the effects of cement content and degree of compaction were highly significant, whereas the effect of stabilizer content was significant. Considering mechanical performance, economy, and deformation-related behavior, the mixture with 6% cement, 0.02% KDJ-II, and 97% compaction was selected for the subsequent comparative tests [21–23]. Therefore, the following comparison between CSS and CPSS was intended to evaluate the early strengthening behavior and microstructural evolution of cement-stabilized soil before and after KDJ-II addition under the selected mixture proportion, rather than to establish a complete dose–response relationship.

To compare the mechanical properties and microstructural evolution of cement-stabilized soil before and after KDJ-II addition, two groups of comparative specimens were prepared: cement-stabilized soil and KDJ-II–cement composite-stabilized soil. The specimens containing only 6% cement with a degree of compaction of 97% were denoted as CSS. The specimens further containing 0.02% KDJ-II on this basis were denoted as CPSS. Both groups of specimens were prepared using cylindrical molds with a diameter of 50 mm and a height of 130 mm, and were compacted using a hydraulic jack. After preparation, the specimens were cured for 1, 3, and 7 days in a standard curing room at 20 ± 1 °C and a relative humidity of at least 90%.

Based on these specimens, early mechanical property tests, XRD, SEM, FTIR, and ion concentration testing were conducted to evaluate the early performance and microstructural evolution of the composite-stabilized soil. For each mechanical index, three replicate specimens were tested for each mixture group. The average value was used as the representative result, and the standard deviation was calculated to evaluate the scatter of the test results. The error bars in Figure 2 represent the standard deviations of the replicate specimens.

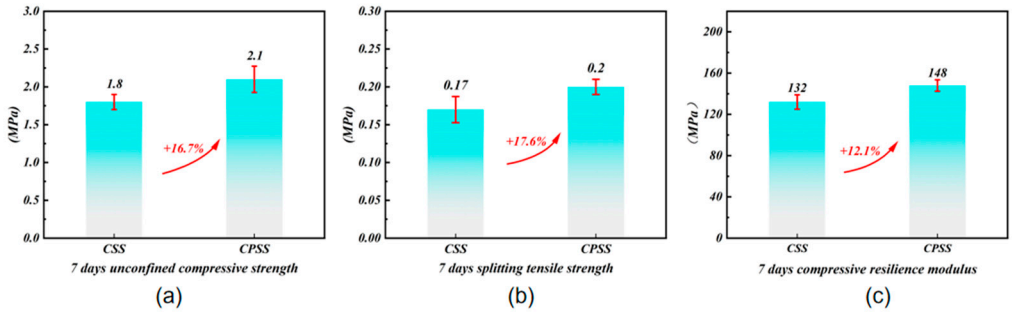

Figure 2. Comparison of early mechanical properties between CSS and CPSS. (**a**) 7-day unconfined compressive strength; (**b**) 7-day splitting tensile strength; (**c**) 7-day compressive resilient modulus. Error bars represent standard deviations.

3. Mechanical Strength Testing of Composite Stabilized Soil

For stabilized soil prepared from loess and intended for use as a base course material, unconfined compressive strength, splitting tensile strength, and resilient modulus are key indicators for evaluating early road performance. These indicators reflect the load-bearing capacity, cracking resistance, and service stiffness of the material, respectively [24]. Therefore, 7-day unconfined compressive strength, splitting tensile strength, and resilient modulus tests were conducted on CSS and CPSS specimens. These tests were used to evaluate the improvement in the early mechanical properties of cement-stabilized soil after the addition of KDJ-II. The results are shown in Figure 2. The values in Figure 2

are presented as mean values, and the error bars represent the standard deviations of three replicate specimens.

As shown in Figure 2, at 7 days, CSS had an unconfined compressive strength of 1.80 ± 0.10 MPa, a splitting tensile strength of 0.17 ± 0.017 MPa, and a compressive resilient modulus of 132 ± 7 MPa. After the addition of 0.02% KDJ-II, the corresponding values of CPSS increased to 2.10 ± 0.17 MPa, 0.20 ± 0.010 MPa, and 148 ± 5.57 MPa, respectively. Compared with CSS, the unconfined compressive strength, splitting tensile strength, and compressive resilient modulus of CPSS increased by 16.7%, 17.6%, and 12.1%, respectively. These results indicate that KDJ-II improved the early strength and stiffness of cement-stabilized soil under the selected mixture proportion and curing condition. However, considering that the comparison was conducted using one selected stabilizer dosage and one cement content, these improvements should be interpreted within the scope of the present experimental conditions.

4. Microstructural Evolution and Stabilization Mechanism

To interpret the possible synergistic stabilization mechanism of cement and KDJ-II, XRD, FTIR, and SEM were used to characterize the mineral phase evolution, bonding environment changes, and microstructural features of CSS and CPSS, respectively. Ion concentration tests at different curing ages were also conducted to analyze the ion release and retention behavior during early strength development in the composite system. Compared with the cement-only system, which is mainly controlled by conventional cement hydration, this study focuses on whether the introduction of KDJ-II is associated with changes in the early reaction environment and product evolution on the basis of conventional cement hydration.

4.1. XRD Analysis of Stabilized Soil

To examine whether the addition of KDJ-II was associated with changes in the phase composition and evolution trend of cement-stabilized soil during early strength development, XRD analysis was conducted on CSS and CPSS specimens. This test was mainly used to identify the crystalline phase composition of the system and its changes. From the perspective of phase evolution, it helped determine whether the composite stabilization system could provide supporting information for possible hydration-related product development, thereby providing a basis for analyzing the strength development mechanism.

4.1.1. XRD Pattern Analysis of Stabilized Soil

CSS and CPSS specimens cured for 1, 3, and 7 days under standard curing conditions were collected. The specimens were crushed, dried, ground, and passed through a 0.075 mm sieve. They were then tested using an X-ray diffractometer. The mineral composition and its evolution were analyzed based on the diffraction peak positions and relative intensities. The results are shown in Figure 3.

Figure 3 shows that the main crystalline phases detected in both CSS and CPSS were quartz, calcite, albite, muscovite, chlorite, and dolomite. The characteristic diffraction peaks of the two groups were generally similar. This result suggests that early curing in both groups involved cement hydration and possible interactions between cementitious products and soil minerals. During this process, hydration products that contributed to strength development may have formed in both systems. These products may include disordered silicate hydration products and sulfate-bearing hydration products. However, because these products usually have low crystallinity and low contents, and because their diffraction peaks can easily overlap with those of original soil minerals and cement-related phases, no clearly distinguishable new characteristic peaks were observed in the XRD

patterns [25,26]. Compared with CSS, the related reaction pathway in CPSS may have changed. However, this difference did not appear as clearly new crystalline phases in terms of mineral type. Instead, it was more likely reflected in the relative contents of different minerals and their evolution trends. Therefore, Rietveld refinement was further used to analyze the mineral composition and changes in relative content of the two groups of specimens.

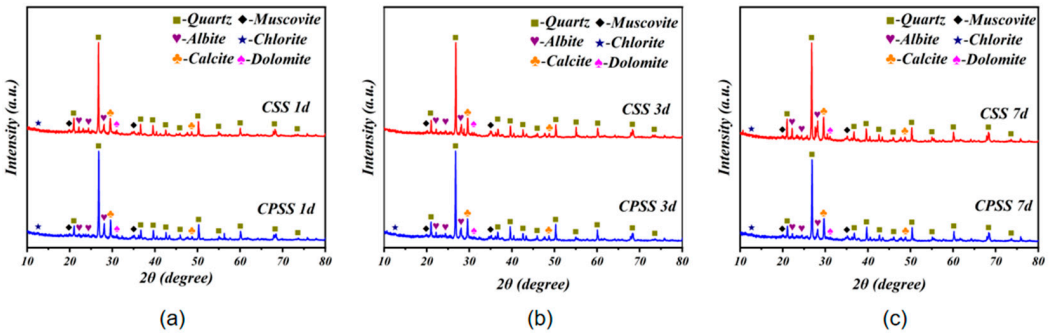

Figure 3. XRD patterns of stabilized soil specimens. (**a**) 1 d; (**b**) 3 d; (**c**) 7 d.

4.1.2. Analysis of Relative Mineral Contents in Stabilized Soil

To analyze the relative contents of crystalline phases in CSS and CPSS, Rietveld refinement was performed on their XRD patterns. The results are shown in Figure 4. It should be noted that the refinement results represent the normalized relative contents of the detected crystalline phases. Therefore, they were mainly used to compare variation trends among different systems and curing ages. These results may also be affected by the formation of amorphous hydration products, such as C–S–H, because no internal standard was used.

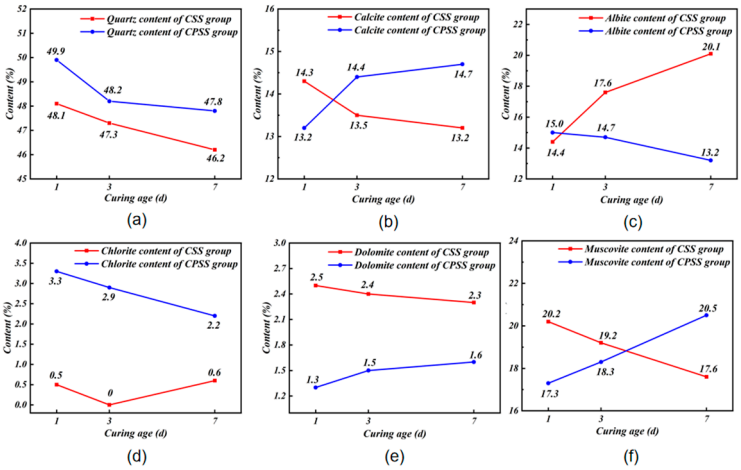

Figure 4. Mineral composition and relative contents of CSS and CPSS: (**a**) quartz; (**b**) calcite; (**c**) albite; (**d**) chlorite; (**e**) dolomite; (**f**) muscovite.

(1) Quartz was the dominant crystalline phase in both groups, and its content decreased only slightly with curing age (CSS: 48.1% → 46.2%; CPSS: 49.9% → 47.8%). The quartz content in CPSS remained slightly higher, by approximately 1.5–1.8%. This can be understood as a relative difference after crystalline-phase normalization. It may also reflect different degrees of amorphous hydration product formation in the two groups.

(2) Calcite showed different variation trends in the two systems. In CSS, the calcite content decreased slightly from 14.3% to 13.2%, which may indicate partial dissolution or consumption of calcite in the alkaline cement environment. In CPSS, the calcite

content increased from 13.2% to 14.7%. This suggests that stronger preservation and/or secondary precipitation, such as carbonation, may have occurred during strength development. The change in calcite may contribute to pore filling and microstructural densification, but its quantitative contribution to strength still needs further verification.

(3) Albite showed opposite trends in the two groups. Its content increased in CSS but decreased in CPSS. This difference may be related to different dissolution–precipitation balances of Na-bearing aluminosilicates in the two systems. It may also be related to normalization effects caused by changes in other crystalline or amorphous components. The change in albite is more likely to reflect the influence of KDJ-II on the early ionic reaction conditions and mineral evolution process of the system. It should not be regarded as direct evidence of a specific recrystallization pathway.

(4) Muscovite decreased in CSS from 20.2% to 17.6%, but increased in CPSS from 17.3% to 20.5%. This difference indicates that composite-stabilized soil was more favorable for preserving the signals of layered silicate minerals, such as muscovite, during early strength development. This may be related to changes in pore-water chemistry and weakened mineral dissolution in the KDJ-II–cement system.

(5) The chlorite content was lower and showed greater fluctuation in CSS, whereas it was higher and more stable in CPSS. For example, the chlorite content in CPSS was approximately 6.6 times that in CSS at 1 day and remained approximately 3.7 times that in CSS at 7 days. This result is consistent with changes in the stability or preservation of Mg-bearing layered silicates in composite-stabilized soil.

(6) Dolomite remained a minor phase throughout the curing period and showed only small changes in both groups. Its content was slightly higher in CSS than in CPSS.

The Rietveld refinement results show that the introduction of KDJ-II influenced the relative proportions and evolution trends of the detected crystalline phases in the composite-stabilized soil. At 7 days, CPSS showed higher relative contents of muscovite and chlorite than CSS, while the relative content of calcite also increased. These changes suggest that KDJ-II may have affected the preservation, dissolution, or precipitation behavior of some primary minerals and Ca-bearing phases during early curing. However, because the refinement results were normalized within the detected crystalline phases and no internal standard was used, these variations should be interpreted as relative trends rather than absolute reaction extents. In addition, low-crystallinity hydration products, such as C–S–H-like gels, could not be directly quantified by this method. Therefore, the XRD results provide supporting evidence for changes in mineral evolution in CPSS, but they should be interpreted together with FTIR, SEM, and leaching-based ion results.

4.2. SEM-Based Microstructural Analysis

To reveal the changes in micro-morphology and pore structure of cement-stabilized soil after the addition of KDJ-II, SEM observations were conducted on CSS and CPSS specimens at different curing ages. This test was mainly used to characterize particle contact modes, pore distribution, and possible gel-like or needle/fibrous products. These observations helped explain the structural basis for the improved strength and stiffness of composite-stabilized soil from the perspective of micro-morphology. The two groups of specimens were sampled after standard curing for 1, 3, and 7 days. After drying, the specimens were tested by scanning electron microscopy (SEM). Microstructural images were obtained at a magnification of 3000×, as shown in Figure 5.

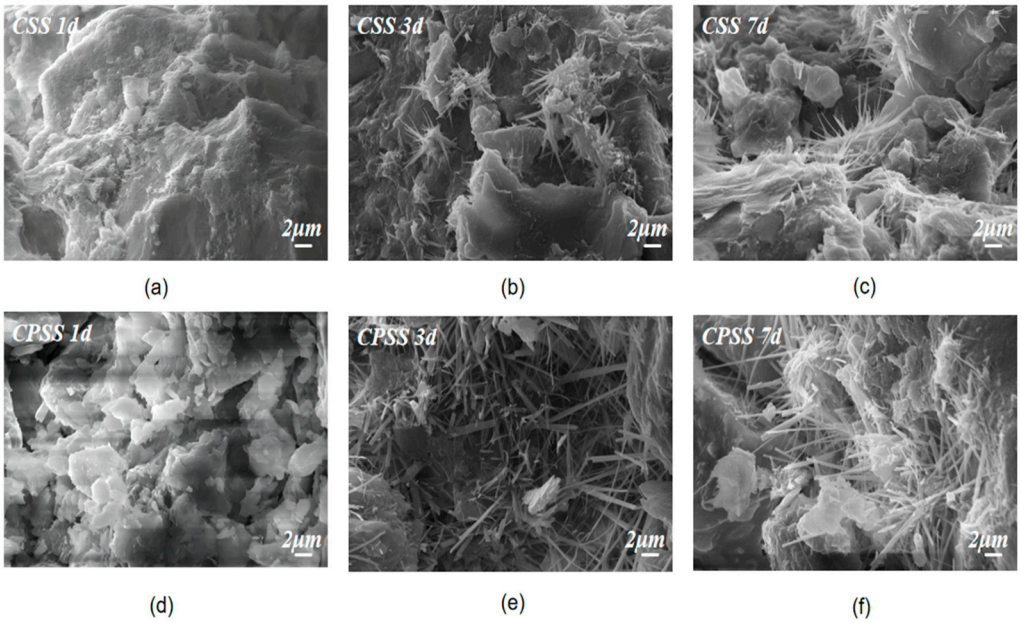

Figure 5. SEM images of the soil microstructure at 3000× magnification. (**a**) CSS, 1 d; (**b**) CSS, 3 d; (**c**) CSS, 7 d; (**d**) CPSS, 1 d; (**e**) CPSS, 3 d; (**f**) CPSS, 7 d.

A comparison of the micro-morphology at 3000× magnification shows that composite-stabilized soil had a denser structure than cement-stabilized soil, with a clear reduction in visible large pores. In cement-stabilized soil, the structural units were mainly connected through point-to-surface and edge-to-surface contacts. In contrast, the structural units in composite-stabilized soil were mostly present as aggregates or stacked forms. The number of pores was clearly reduced, and the contact modes between units were mainly surface-to-surface and edge-to-surface contacts. This indicates that the addition of KDJ-II helped optimize the pore structure and particle contact modes. It also provided microstructural support for the increase in unconfined compressive strength and compressive resilient modulus of composite-stabilized soil.

In addition, clear slender needle/fibrous features with an interlaced distribution were observed in composite-stabilized soil. In contrast, no obvious similar structures were observed in cement-stabilized soil. In composite-stabilized soil, a large amount of material was attached to the surfaces of some mineral particles. Some particle outlines remained relatively clear, whereas others were covered or filled by flocculent materials. By contrast, the mineral surfaces in cement-stabilized soil were relatively smooth, with fewer attachments and clearer particle boundaries. The needle/fibrous features observed in composite-stabilized soil were morphologically similar to AFt-related sulfate-bearing hydration products. The large amount of amorphous flocculent material may be related to C–S–H-like gels [16,17,27]. Together, these two types of products may form an interlaced micro-network structure, thereby enhancing particle bridging and interparticle cementation.

In summary, the combined use of KDJ-II and cement was associated with a denser microstructure, fewer visible large pores, and closer particle contacts in CPSS than in CSS. The needle/fibrous features observed in CPSS were morphologically similar to AFt-related sulfate-bearing hydration products, while the flocculent materials may be associated with C–S–H-like gels. However, because these assignments were based mainly on SEM morphology, they should be regarded as morphological interpretations rather than direct phase identification. Further confirmation using EDS or other targeted microchemical analyses would be needed. Because quantitative image analysis was not performed, the SEM results were used mainly as qualitative morphological evidence. Quantitative pore-size distribution, porosity, and particle-contact statistics should be further investigated in

future work. Nevertheless, the SEM observations support the interpretation that KDJ-II contributed to particle bridging, pore filling, and interparticle cementation, which provides a microstructural explanation for the improved early strength and stiffness of CPSS under the tested conditions.

4.3. FTIR Spectroscopy Analysis of Micro-Solidification Mechanism

To analyze the changes in the bonding environment of cement-stabilized soil during early strength development after the addition of KDJ-II, FTIR tests were conducted on CSS and CPSS specimens. This test was mainly used to characterize the changes in silicate-, carbonate-, and hydroxyl-related functional groups in composite-stabilized soil. From the perspective of the bonding environment, it helped assess the development of substances such as disordered silicate hydration products and provided supplementary evidence for the analysis of the micro-solidification mechanism. Specimens of the two groups were collected after standard curing for 1, 3, and 7 days. After drying, crushing, and grinding, the specimens were tested using Fourier-transform infrared spectroscopy (FTIR). Infrared spectra in the range of 400–4000 cm^{-1} were obtained, as shown in Figure 6.

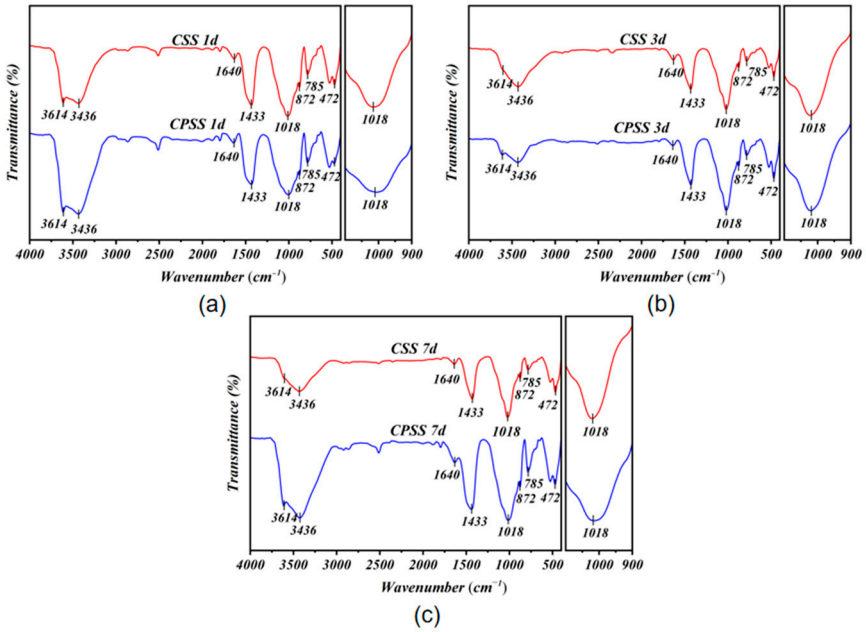

Figure 6. FTIR spectra of CSS and CPSS. (**a**) 1 d; (**b**) 3 d; (**c**) 7 d.

As shown in Figure 6, the overall spectral profiles of CSS and CPSS were relatively similar. This indicates that the two systems had generally similar bonding environments during early strength development. The broad peak at approximately 3436 cm^{-1} and the absorption band at approximately 1640 cm^{-1} correspond to O–H stretching vibration and H–O–H bending vibration, respectively. This indicates the presence of physically adsorbed water and/or bound water in both systems. The absorption band at approximately 1433 cm^{-1} is usually associated with carbonate-related vibrations. It may originate from the carbonation of $Ca(OH)_2$ and/or carbonate-containing phases in the cement system [28]. Its presence is consistent with the calcite variation trend observed by XRD. The broad peak at approximately 1018 cm^{-1} is assigned to Si–O–T (T = Si or Al) stretching vibration. It reflects the bonding environment of the aluminosilicate/silicate network. Compared with CSS, CPSS showed a larger full width at half maximum for this peak. This may indicate a wider distribution of Si–O–T bonding environments and a higher degree of structural disorder. This type of peak broadening is often related to the development of amorphous hydration products, such as C–S–H-like gels [27,29].

Overall, the FTIR results indicate that the addition of KDJ-II was associated with changes in silicate- and carbonate-related bonding environments during early curing. In particular, the broadening of the absorption band at approximately 1018 cm^{-1} in CPSS supports the interpretation that disordered or amorphous silicate hydration products, such as C–S–H-like gels, may have developed more actively in the composite system. However, because no peak deconvolution or quantitative FTIR analysis was performed, this result should be interpreted as qualitative supporting evidence rather than direct quantification of hydration products. Together with the XRD and SEM observations, the FTIR results suggest that KDJ-II may have promoted the development of hydration-related products and microstructural densification on the basis of conventional cement hydration.

4.4. Analysis of the Stabilization Mechanism Based on Ion Concentration Changes

To further analyze the early ion release and retention behavior of composite-stabilized soil after the introduction of KDJ-II, leaching-based ion concentration tests were conducted on CSS and CPSS specimens at different curing ages. It should be noted that the measured ion concentrations represent the ions released into purified water under the specified extraction condition, rather than the in-situ pore-solution chemistry during curing. Therefore, the leaching results were used to compare the relative ion release, retention, and solid–liquid partitioning behavior of the two systems, rather than to directly quantify pore-solution composition or reaction stoichiometry. Early strength development in both cement-stabilized soil and composite-stabilized soil was mainly based on cement hydration and the cementation of soil particles. Compared with CSS, the addition of KDJ-II introduced sulfate-, sodium-, and silicate-related components into the system, which may have influenced the leachable ion environment and provided conditions favorable for subsequent hydration-related reactions. Specimens of the two groups were collected after standard curing for 1, 3, and 7 days and were then used for leaching-based ion concentration tests. During testing, each specimen was immersed in purified water at a solid-to-liquid ratio of 1:10 and kept at 25 ± 1 °C for 24 h. The mixture was then filtered, and the clear leachate was collected for ion concentration analysis. The results are shown in Figures 7–11.

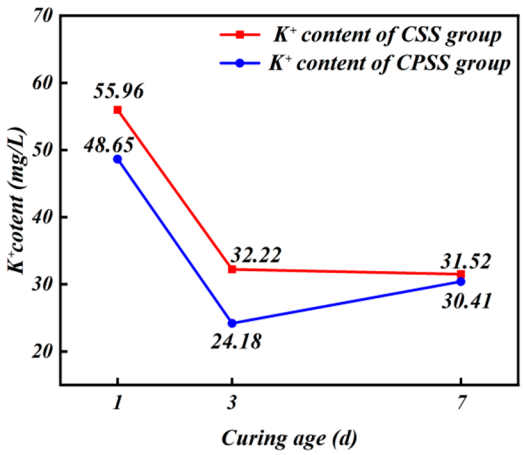

Figure 7. Variation in K^+ concentration with curing age.

Figures 7 and 8 show the variation trends of leachable K^+ and Mg^{2+} concentrations with curing age, respectively. As shown in Figure 7, CPSS showed a lower leachable K^+ concentration than CSS during early curing. This may indicate that part of the K^+ was retained in the solid phase, incorporated into newly formed hydration-related products, or adsorbed on mineral surfaces, thereby reducing its release into the leachate. Figure 8 shows that CPSS had a relatively low leachable Mg^{2+} concentration at the early stage, which may

be related to the reduced dissolution of Mg-bearing phases or the enhanced retention of Mg^{2+} in the solid phase. The later increase in Mg^{2+} concentration may reflect redistribution between the solid and liquid phases during curing and extraction. Overall, the changes in K^+ and Mg^{2+} mainly indicate differences in ion release and solid–liquid partitioning behavior between CSS and CPSS. These changes alone are not sufficient to define a specific reaction pathway, but they provide supporting evidence for the modified leachable ion environment in the composite system.

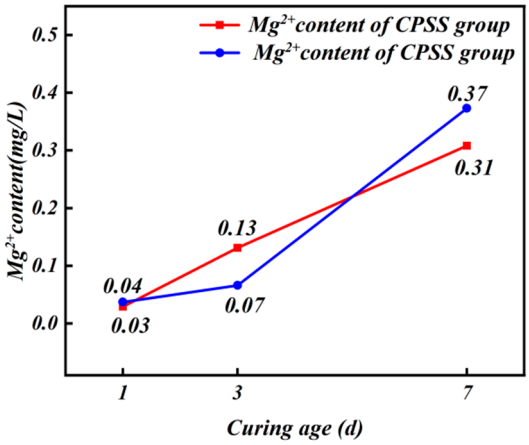

Figure 8. Variation in Mg^{2+} concentration with curing age.

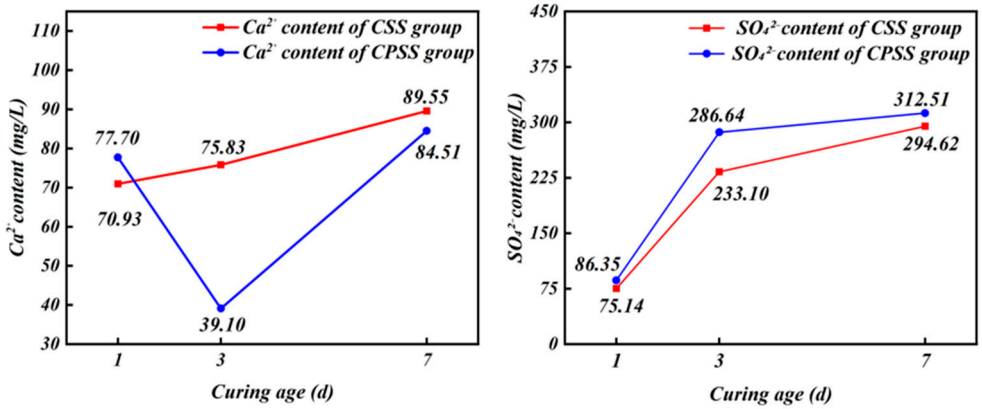

Figure 9. Variation in Ca^{2+} and $SO_4{}^{2-}$ concentrations with curing age.

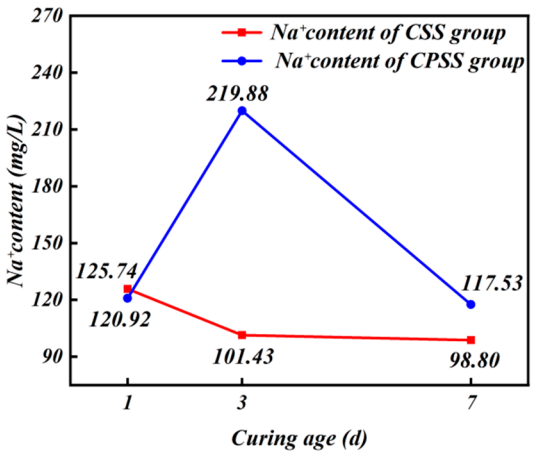

Figure 10. Variation in Na^+ concentration with curing age.

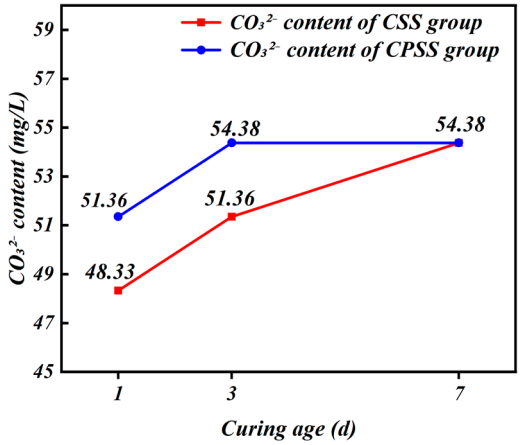

Figure 11. Variation in CO_3^{2-} concentration with curing age.

In comparison, the coupled variations in leachable Ca^{2+} and SO_4^{2-} provide useful information for understanding the early reaction tendency of the composite system. As shown in Figure 9, CPSS generally exhibited a higher leachable SO_4^{2-} concentration and a lower leachable Ca^{2+} concentration than CSS. The higher SO_4^{2-} concentration should first be attributed to the sulfate introduced by KDJ-II. At the same time, the sulfate-rich environment may provide favorable chemical conditions for the development of sulfate-bearing hydration products. For the cement-only system, the variation in Ca^{2+} was mainly associated with conventional cement hydration and the formation of cementitious products. In CPSS, the lower leachable Ca^{2+} concentration may reflect stronger Ca^{2+} retention or consumption in the solid phase, which could be related to the formation of cementitious products and possibly sulfate-bearing hydration products. Combined with the needle/fibrous features observed by SEM, the ion concentration results support the interpretation that AFt-related products may have developed more actively in the composite system, although direct identification would require additional evidence such as EDS or more targeted phase analysis. To improve notation consistency, the following equations are presented as schematic reaction pathways. They are used to illustrate possible reaction tendencies rather than to provide complete stoichiometric or thermodynamic descriptions of the stabilized soil system.

$$3CaO{\cdot}Al_2O_3(s) + 3CaSO_4(aq/s) + 32H_2O(l) \rightarrow 3CaO{\cdot}Al_2O_3{\cdot}3CaSO_4{\cdot}32H_2O(s)\ (AFt) \quad (1)$$

Equation (1) is a simplified representation of the possible formation of AFt-related sulfate-bearing hydration products. It does not indicate that AFt was quantitatively identified in the present system. Instead, the higher leachable SO_4^{2-} concentration, the variation in leachable Ca^{2+}, and the SEM-observed needle/fibrous morphology jointly support the possible development of AFt-related products in CPSS.

In addition to sulfate-related reactions, Na^+ variation provides another indication of the modified leachable ion behavior in CPSS. As shown in Figure 10, CPSS showed a transient Na^+ peak at 3 days. This peak should be interpreted cautiously because Na^+ may originate from both the Na-bearing components introduced by KDJ-II and the dissolution of Na-bearing aluminosilicate minerals in loess. Therefore, the Na^+ peak cannot be assigned solely to albite dissolution. Nevertheless, when this result is considered together with the decrease in the relative content of albite observed by XRD, it supports the interpretation that the alkaline environment associated with KDJ-II may have promoted the partial dissolution or activation of Na-bearing aluminosilicate minerals. This process may release reactive Si and Al species that could participate in subsequent hydration-related reactions. The

possible dissolution of albite under alkaline conditions can be expressed in a simplified form as follows:

$$NaAlSi_3O_8(s) + 8H_2O(l) \rightarrow Na^+(aq) + Al(OH)_4^-(aq) + 3H_4SiO_4(aq) \quad (2)$$

Equation (2) illustrates a possible dissolution pathway of albite under aqueous alkaline conditions. However, because Na^+ in CPSS may originate from both KDJ-II and Na-bearing aluminosilicate minerals, the observed Na^+ fluctuation should not be assigned solely to albite dissolution. Rather, it should be interpreted as indirect evidence that KDJ-II may have influenced the participation of Na-bearing aluminosilicate minerals in the early reaction process.

Figure 11 shows that the leachable CO_3^{2-} concentration tended to stabilize after 3 days. This trend was generally consistent with the relatively gentle variation in calcite observed by XRD refinement. It indicates that carbonate-related processes existed in the system, but they were not the dominant factor controlling the early reaction behavior of CPSS. In comparison, the combined effect of soluble silica introduced by KDJ-II and reactive silica possibly released from aluminosilicate minerals may have provided favorable conditions for the development of low-crystallinity silicate hydration products. Ca^{2+} released during cement hydration could react with dissolved silicate species to form C–S–H-like gels [30,31]. This process can be simplified as follows:

$$xCa^{2+}(aq) + yH_4SiO_4(aq) + zOH^-(aq) + nH_2O(l) \rightarrow C–S–H\ gel(s) \quad (3)$$

Equation (3) is a schematic expression for the possible formation of C–S–H-like gels from calcium and dissolved silicate species. It should not be regarded as a balanced stoichiometric equation. The FTIR band broadening near 1018 cm^{-1} and the flocculent gel-like materials observed by SEM support the possible development of low-crystallinity silicate hydration products, but further quantitative phase analysis would be required for direct confirmation.

Based on Figures 7–11, the leaching-based ion concentration changes in CPSS should be understood as interrelated indicators of ion release, retention, and solid–liquid partitioning behavior. Compared with CSS, the addition of KDJ-II introduced sulfate-, sodium-, and silicate-related components and modified the early leachable ion environment. These changes may have provided favorable conditions for sulfate-bearing hydration product development, partial activation of aluminosilicate minerals, and the formation of C–S–H-like gels. However, because the ion test was based on water extraction rather than direct pore-solution measurement, these results should be regarded as indirect evidence supporting the proposed reaction pathway. When combined with XRD, FTIR, and SEM observations, the leaching-based ion results support the interpretation that KDJ-II promoted particle cementation, pore filling, and microstructural densification, thereby contributing to the higher early strength and stiffness of CPSS under the tested conditions.

4.5. Stabilization Mechanism

Based on the integrated evidence from XRD, SEM, FTIR, and leaching-based ion concentration analysis, Figure 12 presents the microstructural evolution and proposed stabilization mechanism of KDJ-II–cement composite-stabilized soil during early strength development.

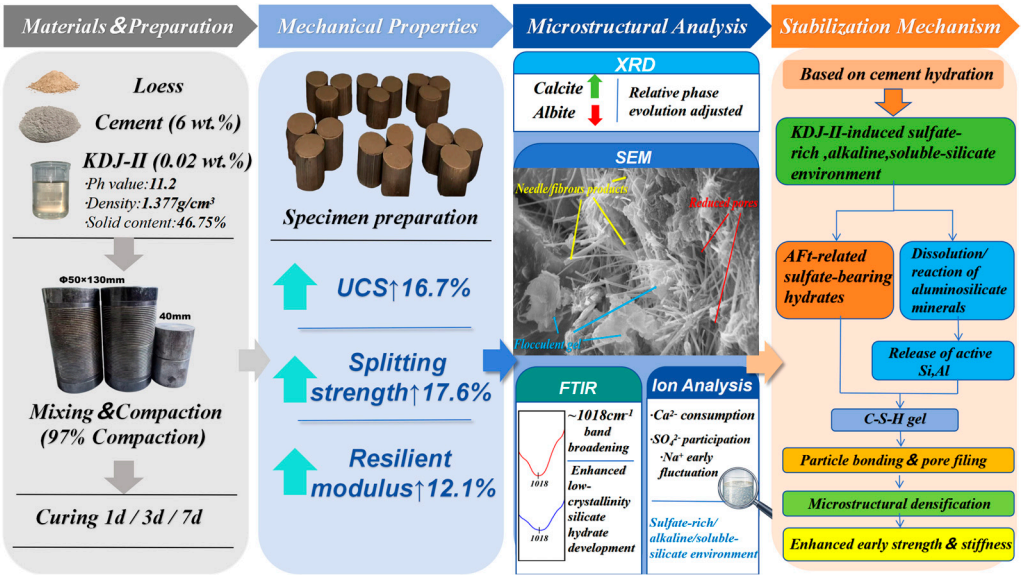

Figure 12. Schematic diagram.

As shown in Figure 12, early strength development in both CSS and CPSS was based on cement hydration and its basic cementation effect. The difference is that the introduction of KDJ-II further formed a sulfate-rich, highly alkaline, and soluble-silica-bearing reaction environment in the composite system on this basis. This environment made the microstructural evolution process more favorable for the continuous development of subsequent products. In this environment, on the one hand, the additional sulfate was favorable for the development of sulfate-bearing hydration products, possibly including AFt-related products. On the other hand, the highly alkaline condition promoted the dissolution–reaction of primary aluminosilicate minerals in loess and provided reactive Si and Al components for the subsequent continuous formation of C–S–H-like gels. As a result, a reaction process developed in composite-stabilized soil. This process was based on conventional cement hydration and further coupled with the development of sulfate-bearing hydration products, mineral activation, and continuous gel formation.

This proposed mechanism is supported by the combined experimental observations. XRD and FTIR provided evidence for changes in mineral evolution and bonding environments, while leaching-based ion results reflected differences in ion release and retention behavior. SEM observations showed needle/fibrous products, flocculent gels, reduced visible pores, and a denser particle arrangement. These observations collectively support the interpretation that KDJ-II was associated with product development and structural densification under the tested conditions.

Overall, the role of KDJ-II should be interpreted as a modification of the early reaction environment under the selected mixture proportion, rather than as the introduction of an entirely independent stabilization mechanism. On the basis of conventional cement hydration, KDJ-II introduced sulfate-, sodium-, and silicate-related components and influenced the leachable ion release and retention behavior of the system. These changes may have favored the development of sulfate-bearing hydration products, partial activation of primary aluminosilicate minerals, and the formation of C–S–H-like gels. As supported by the SEM observations, these processes were associated with enhanced particle contact, pore filling, and microstructural densification. Therefore, the proposed mechanism provides a reasonable explanation for the improved early strength and stiffness of CPSS under the tested conditions, although further direct phase identification and durability tests are still required.

It should also be noted that this study focused on the early-age behavior of one low-plasticity loess treated with one cement content and one selected KDJ-II dosage under standard curing conditions. Therefore, the proposed mechanism should be regarded as applicable to the tested material and curing conditions rather than as a universal conclusion for all loess soils or field environments. In addition, long-term strength development and durability-related properties, such as water stability, wetting–drying resistance, freeze–thaw durability, erosion resistance, and shrinkage behavior, were not evaluated in this study. These aspects should be further investigated before the composite-stabilized soil is applied more broadly as a pavement base-course material.

5. Conclusions

This study evaluated the early mechanical properties and microstructural evolution of cement-stabilized soil with and without KDJ-II. XRD, SEM, FTIR, and leaching-based ion concentration analyses were used to interpret the possible early strength development mechanism. The results indicate that, under the selected mixture proportion and curing condition, the addition of KDJ-II improved the early strength and stiffness of cement-stabilized soil. The leaching-based ion results, together with the XRD, FTIR, and SEM observations, support the interpretation that KDJ-II influenced the early ion release and retention behavior and promoted particle cementation, pore filling, and microstructural densification. The main conclusions are as follows:

(1) Compared with cement-stabilized soil, the introduction of KDJ-II improved the early mechanical properties of the stabilized soil under the selected mixture proportion. At 7 days, the unconfined compressive strength, splitting tensile strength, and resilient modulus increased by 16.7%, 17.6%, and 12.1%, respectively. These results indicate that the composite-stabilized soil developed a more favorable cemented and densified structure at an early age, thereby improving the load-bearing capacity, cracking resistance, and stiffness of the material. However, these improvements should be interpreted within the tested loess type, cement content, KDJ-II dosage, and curing condition.

(2) The variations in leachable Ca^{2+}, $SO_4{}^{2-}$, and Na^{+} indicate that KDJ-II influenced the early ion release, retention, and solid–liquid partitioning behavior of cement-stabilized soil. The higher leachable $SO_4{}^{2-}$ concentration in CPSS was mainly related to the sulfate introduced by KDJ-II, while the variation in leachable Ca^{2+} may reflect a dynamic balance among cement hydration, dissolution, precipitation, and solid-phase retention. The transient Na^{+} peak may be associated with both the Na-bearing components introduced by KDJ-II and the partial dissolution or activation of Na-bearing aluminosilicate minerals. Therefore, the ion concentration results should be regarded as indirect evidence supporting the proposed reaction pathway rather than as direct pore-solution evidence.

(3) XRD and FTIR provided supporting evidence for changes in mineral phase evolution and bonding environments during early curing. The Rietveld refinement results showed an increase in the relative calcite content and a decrease in the relative albite content in CPSS. Because the refinement results were normalized within the detected crystalline phases and no internal standard was used, these changes should be interpreted as relative trends rather than absolute reaction extents. The decrease in albite, together with the Na^{+} fluctuation, suggests that KDJ-II may have promoted the partial activation of Na-bearing aluminosilicate minerals. The broadening of the absorption band at approximately 1018 cm^{-1} in the FTIR spectra further supports the possible development of disordered silicate hydration products, such as C–S–H-like gels.

(4) SEM observations showed that CPSS had more needle/fibrous features, flocculent gel-like materials, reduced visible pores, and closer particle contacts than CSS. The needle/fibrous features may be related to AFt-related sulfate-bearing hydration products, while the flocculent materials may be associated with C–S–H-like gels. These microstructural observations support the interpretation that KDJ-II promoted particle bridging, interparticle cementation, pore filling, and structural densification. Such microstructural refinement provides a reasonable explanation for the improved early strength and stiffness of CPSS under the tested conditions.

Author Contributions: Conceptualization, H.W., B.Z., X.N., W.Z. and Y.T.; formal analysis, H.W., B.Z., X.N., W.Z., Y.T. and C.C.; investigation, H.W. and Y.T.; methodology, R.W.; data curation, R.W.; writing—original draft preparation, R.W.; visualization, R.W.; writing—review and editing, R.W. and W.Z. All authors have read and agreed to the published version of the manuscript.

Funding: This research was funded by the Research Project of Gansu Provincial Department of Transportation, grant number 2024-08; the National Natural Science Foundation of China, grant number 42562035; the Key Research and Development Program of Gansu Province, grant number 25YFGA014.

Institutional Review Board Statement: Not applicable.

Informed Consent Statement: Not applicable.

Data Availability Statement: The data underlying this article will be shared upon reasonable request to the corresponding author.

Acknowledgments: The authors thank the Gansu Key Laboratory of Green Engineering Materials and Low-Carbon Construction for providing experimental facilities.

Conflicts of Interest: Author Chenggui Chen was employed by the company Gansu Provincial Transportation Research Institute Group Co., Ltd. The remaining authors declare that the research was conducted in the absence of any commercial or financial relationships that could be construed as a potential conflict of interest.

Abbreviations

The following abbreviations are used in this manuscript:

CPSS	KDJ-II–Cement Composite-Stabilized Soil
CSS	Cement-Stabilized Soil
XRD	X-ray Diffraction
SEM	Scanning Electron Microscope
FTIR	Fourier Transform Infrared Spectroscopy

References

1. Ren, Z.; Jiang, M.; Behrens, P.; Chen, D.; Mostert, C.; Zhou, W.; Li, C.; Li, F.; Liu, L.; Wang, H.; et al. Declining demand and circular transition possibilities of sand, gravel and crushed stone in China. *Nat. Commun.* **2025**, *16*, 9294. [CrossRef]
2. Li, G.; Wang, F.; Ma, W.; Fortier, R.; Mu, Y.; Mao, Y.; Hou, X. Variations in strength and deformation of compacted loess exposed to wetting-drying and freeze-thaw cycles. *Cold Reg. Sci. Technol.* **2018**, *151*, 159–167. [CrossRef]
3. Yuan, K.; Wang, H.; Ni, W.; Ren, S.; Guo, Y. New insights into the dynamic changes of loess collapsibility under climate-induced wetting-drying cycles: A case study of the Loess Plateau of China. *Catena* **2025**, *250*, 108782. [CrossRef]
4. Tian, L.; Bao, W.; Huang, Z.; Zhang, Z. Macro/microstructure deterioration mechanism and constitutive modeling of compacted loess under drying-wetting-freezing-thawing cycles. *Eng. Geol.* **2025**, *359*, 108442. [CrossRef]
5. Jiang, Y.J.; Ni, C.Y.; Sha, H.W.; Li, Z.H.; Cai, L.Y. Deterioration characteristics of cement-improved loess under dry-wet and freeze-thaw cycles. *PLoS ONE* **2021**, *16*, e0253199. [CrossRef]

6. Zhu, W.; Long, Z.; He, L.; Ye, S.; Mao, Y. Hydro-physical properties and durability study of cement slurry material based on loess. *Sci. Rep.* **2025**, *15*, 13198. [CrossRef]
7. Yangsukkasem, N.; Suebsuk, J.; Kampala, A.; Siriphan, A.; Somna, R.; Jiammeepreecha, W.; Chindaprasirt, P. Durability against cyclic wetting-drying of cement-stabilized loess subgrade for railway in tropical semi-arid regions. *Constr. Build. Mater.* **2024**, *455*, 139123. [CrossRef]
8. Wu, Z.; Liu, Y.; Intaj, F. Minimizing Shrinkage Cracking in Cement-Stabilized Bases Through Micro-Cracking. FHWA/LA.18/588 Final Report, 2018. Available online: https://rosap.ntl.bts.gov/view/dot/61444 (accessed on 2 June 2026).
9. Al-Dakheeli, H.; Arefin, S.; Bulut, R.; Little, D. Effectiveness of ionic stabilization in the mitigation of soil volume change behavior. *Transp. Geotech.* **2021**, *29*, 100573. [CrossRef]
10. Greening, P.A.K.; Page-Green, P. Evaluation of Sulphonated Petroleum Products as Soil Stabilisers and Compaction Aids. TRL/CSIR Report, Project R6896, 2003. Available online: https://assets.publishing.service.gov.uk/media/57a08d0eed915d622c001747/R6896.pdf (accessed on 2 June 2026).
11. Lu, J.; Jiang, S.Y.; Chen, J.; Lee, C.H.; Cai, Z.; Ruan, H.D. Fabrication of superhydrophobic soil stabilizers derived from solid wastes applied for road construction: A review. *Transp. Geotech.* **2023**, *40*, 100974. [CrossRef]
12. Jia, J.; Lu, X.; Zhu, J.; Wang, J.; Zhang, L.; Cheng, X. Effect of ionic soil stabilizer on the properties of lime and fly ash stabilized iron tailings as pavement base. *Constr. Build. Mater.* **2024**, *450*, 138558. [CrossRef]
13. Li, H.; Jia, J.; Lu, X.; Cheng, X.; Zhu, J.; Zhang, L.; Guo, P.; Zhai, G. The effect of ionic soil stabilizer on cement and cement-stabilized iron tailings soil: Hydration difference and mechanical properties. *Materials* **2025**, *18*, 1444. [CrossRef] [PubMed]
14. Li, G.; Ren, Z.; Liu, J.; Chen, H.; Wen, Z.; Fu, C. Enhancing coastal saline dispersive soil with ionic stabilizer-cement synergy: Mechanisms and performance. *Case Stud. Constr. Mater.* **2025**, *23*, e05519. [CrossRef]
15. Barbieri, D.M.; Lou, B.; Dyke, R.J.; Wang, X.; Chen, H.; Shu, B.; Gazder, U.; Horpibulsuk, S.; Tingle, J.S.; Hoff, I. Design and sustainability analyses of road base layers stabilized with traditional and nontraditional additives. *J. Clean. Prod.* **2022**, *372*, 133752. [CrossRef]
16. Santoni, R.L.; Tingle, J.S.; Webster, S.L. Stabilization of silty sand with nontraditional additives. *Transp. Res. Rec.* **2002**, *1787*, 61–70. [CrossRef]
17. Tingle, J.S.; Newman, J.K.; Larson, S.L.; Weiss, C.A.; Rushing, J.F. Stabilization mechanisms of nontraditional additives. *Transp. Res. Rec.* **2007**, *1989*, 59–67. [CrossRef]
18. Wang, Q.; Li, Y.; Li, P.; Qi, Y. Using cement and calcium lignosulfonate to improve the mechanical properties and microstructure of loess in a seasonal freezing zone. *Buildings* **2024**, *14*, 1495. [CrossRef]
19. Julphunthong, P.; Joyklad, P.; Manprom, P.; Chompoorat, T.; Palou, M.-T.; Suriwong, T. Evaluation of calcium carbide residue and fly ash as sustainable binders for environmentally friendly loess soil stabilization. *Sci. Rep.* **2024**, *14*, 671. [CrossRef]
20. Yuan, K.; Ni, W.; Zhao, L.; Wang, H. Silica fume stabilized loess: Mechanical properties, microstructural evolution and environmental analysis. *Sustain. Mater. Technol.* **2023**, *36*, e00604. [CrossRef]
21. *JTG 3430-2020*; Test Methods of Soils for Highway Engineering. Ministry of Transport of the People's Republic of China: Beijing, China, 2020.
22. *JTG 3441-2024*; Test Methods of Materials Stabilized with inorganic Binders for Highway Engineering. Ministry of Transport of the People's Republic of China: Beijing, China, 2024.
23. Jiao, S. Application Research of Composite Stabilized Loess in Base Courses of Low-Grade Highways. Master's Thesis, Northwest Minzu University, Lanzhou, China, 2024.
24. Chang, J.; Li, J.; Wang, Y.; Zhang, H. Mechanical characteristics and microstructural changes in phosphogypsum-cement-lime composite modified loess. *Case Stud. Constr. Mater.* **2024**, *21*, e03881. [CrossRef]
25. de Matos, P.R.; Andrade Neto, J.S.; Sakata, R.D.; Kirchheim, A.P.; Rodríguez, E.D.; Campos, C.E.M. Strategies for XRD quantitative phase analysis of ordinary and blended Portland cements. *Cem. Concr. Compos.* **2022**, *131*, 104571. [CrossRef]
26. de Matos, P.R.; Andrade Neto, J.S.; Jansen, D.; De la Torre, A.G.; Kirchheim, A.P.; Campos, C.E.M. In-situ laboratory X-ray diffraction applied to assess cement hydration. *Cem. Concr. Res.* **2022**, *162*, 106988. [CrossRef]
27. Yang, X.; Hu, Z.; Li, L.; Wang, X.; Zhou, X. Strength properties, microstructural evolution, and reinforcement mechanism for cement-stabilized loess with silica micro powder. *Case Stud. Constr. Mater.* **2024**, *20*, e02848. [CrossRef]
28. Ylmén, R.; Jäglid, U. Carbonation of Portland cement studied by diffuse reflection FTIR spectroscopy. *Int. J. Concr. Struct. Mater.* **2013**, *7*, 119–125. [CrossRef]
29. Yusuf, M.O. Bond characterization in cementitious material binders using Fourier-transform infrared spectroscopy. *Appl. Sci.* **2023**, *13*, 3353. [CrossRef]

30. Bernard, E.; Yan, Y.; Lothenbach, B. Effective cation exchange capacity of calcium silicate hydrates (C-S-H). *Cem. Concr. Res.* **2021**, *143*, 106393. [CrossRef]
31. Yan, Y.; Bernard, E.; Miron, G.D.; Rentsch, D.; Ma, B.; Scrivener, K.; Lothenbach, B. Kinetics of Al uptake in synthetic calcium silicate hydrate (C-A-S-H). *Cem. Concr. Res.* **2023**, *172*, 107296. [CrossRef]